

The nine ways of four-qubit entanglement and their threetangle

Andreas Osterloh

*Institut für Theoretische Physik, Universität Duisburg-Essen, D-47048 Duisburg, Germany.**

I calculate the mixed threetangle $\tau_3[\rho]$ for the reduced density matrices of the four-qubit representative states found in Phys. Rev. A **65**, 052112 (2002). In most of the cases, the convex roof is obtained, except for one class, where I provide with a new upper bound, which is assumed to be very close to the convex roof. I compare with results published in Phys. Rev. Lett. **113**, 110501 (2014). Since the method applied there usually results in higher values for the upper bound, in certain cases it can be understood that the convex roof is obtained exactly, namely when the zero-polytope where τ_3 vanishes shrinks to a single point.

INTRODUCTION

Entanglement has become a central part of modern physics and hence, also quantifying this physical resource has gained much relevance. For two qubits, only one class of entanglement exists, and its entanglement could also be determined exactly using the concurrence[1, 2]. Every entanglement measure that is extended from pure to mixed states by means of the convex roof construction[3] can be written as a function of this measure. A bit later, the threetangle[4] was extracted as the residual tangle of a monogamy relation for pure three qubit states[4, 5]. This was the first entanglement measure that could distinguish in a sharp way the two different ways three qubits can be entangled[6]. This is a task which is only achievable by an SL -invariant entanglement measure, instead of incorporating the minimal unitary symmetry of entanglement[7]. Examples for the latter are entanglement measures connected to the partial transpose criterion[8–11]. It was only later that the relevance of the invariance with respect to the group SL became clearer to the community[6, 12–18]. Unfortunately, the convex roof extension to mixed states seems difficult in view of the infinitely many decompositions of a density matrix ρ , and the first solutions to the convex roof of the threetangle emerged therefore only for special symmetric states[19–22]. A considerable advance was the lower bound of the threetangle in terms of that of the GHZ symmetrized version of the state. The convex roof of the square root of the threetangle[12, 23] of the latter could be calculated exactly[24, 25] in the same way as outlined in Ref. [19, 20]. Recently, a code was invented that upper bounds arbitrary SL invariant entanglement measure E for density matrices of variable rank[26], by considering the manifold made of the extreme points of the zero-polytopes[33], and measuring the distance to the barycenter of these points. This method has been applied for making statements about the residual tangle in pure states of four qubits[27]. This work fills the gap, proclaimed in this latter reference, namely of providing with an atlas of the threetangle for the existing classification of four-qubit pure states[12].

This article is laid out as follows. In the following

section, I review relevant subjects of how convex roofs can be obtained and the connection to what is called *characteristic curves*[19, 20]. In the sequel, I will treat each different class of $SL(2)^{\otimes 4}$ separately and calculate the convex roof, except for one class, where an upper bound is obtained. At the end, I make some concluding remarks.

MINIMAL CHARACTERISTIC CURVE AND CONVEX ROOF

Let E denote the entanglement measure, and let it be a homogenous polynomial SL invariant of degree $D = 2n$ for integers n . The entanglement of a rank two density matrix

$$\rho = \sum_{i=1}^2 p_i |\psi_i\rangle\langle\psi_i| ; \langle\psi_i|\psi_j\rangle = \delta_{ij} \quad (1)$$

can only be made out of pure states in its range

$$|\Psi(p_1; \varphi)\rangle = \sqrt{p_1}|\psi_1\rangle + \sqrt{p_2}e^{i\varphi}|\psi_2\rangle . \quad (2)$$

These states are best visualized on a Bloch sphere (see Fig. 1). In order to calculate the convex roof, we have to analyze the entanglement $E(|\Psi(p_1; \varphi)\rangle)$ for all such states. This corresponds to looking at[19, 20]

$$E(|\Psi(z)\rangle) = E(|\psi_1\rangle + z|\psi_2\rangle) , \quad (3)$$

where the p_i are functions of z : $p_1 = 1/(1 + |z|^2)$ and $p_2 = |z|^2/(1 + |z|^2)$. The characteristic curves for E are $E(|\Psi(p_1; \varphi)\rangle) = E(|\Psi(z)\rangle)$ and their minimum (which may depend explicitly on φ)

$$E_{\min}(p) := \min_{\varphi} \{E(|\Psi(p; \varphi)\rangle)\} \quad (4)$$

are of utmost importance for the determination of $E(\rho)$ [19, 20]. I have relaxed the definition of the characteristic curve of Ref. [19, 20] slightly: the minimal characteristic curve $E_{\min}(p)$ here is the characteristic curve in Ref. [19, 20].

Whereas in general one will find an explicit phase dependence $p(\varphi)$ in E_{\min} , here we have given values for

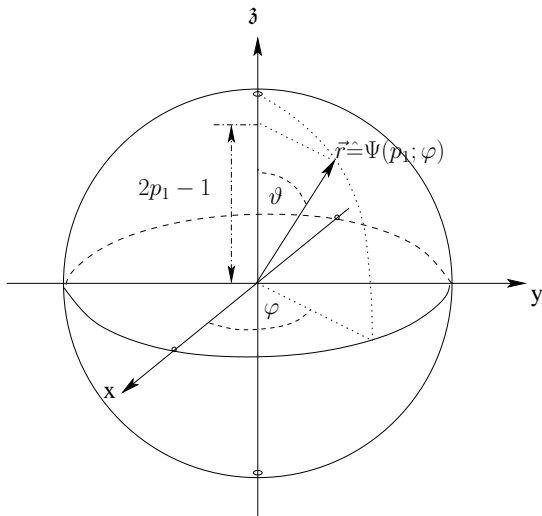


FIG. 1: The Bloch sphere with radius $|\vec{r}| = 1$ and the standard parametrization of its surface in the angles ϑ and φ of the vector \vec{r} . This vector corresponds to the pure state $|\Psi(p_1; \varphi)\rangle = \cos \frac{\vartheta(p_1)}{2} |\psi_1\rangle + \sin \frac{\vartheta(p_1)}{2} e^{i\varphi} |\psi_2\rangle = \sqrt{p_1} |\psi_1\rangle + \sqrt{1-p_1} e^{i\varphi} |\psi_2\rangle$. The r_3 component is related to the probability p_1 via $r_3 = 2p_1 - 1$.

$\varphi = \varphi_0$ for which the minimum is achieved. If a decomposition is found whose entanglement lies on the convexified minimal characteristic curve, then this decomposition is certainly optimal[19, 20] and the convex roof is obtained. In general it is a solution which lies above the convexification of E_{\min} .

We need to consider solutions to the zero-polytope made out of the solutions to

$$E\left(\frac{|\psi_1\rangle}{\|\psi_1\|} + z \frac{|\psi_2\rangle}{\|\psi_2\|}\right) = 0 \quad (5)$$

and define

$$|\Psi_z\rangle := \sqrt{p_1(z)} \left(\frac{|\psi_1\rangle}{\|\psi_1\|} + z \frac{|\psi_2\rangle}{\|\psi_2\|} \right) \quad (6)$$

and the probability $p_1(z)$ of $|\psi_1\rangle$ is

$$p_1(z) = \frac{1}{1 + |z|^2}. \quad (7)$$

The zero-polytope is made out of as many pure states as the homogeneous degree of E . For $E = \tau_3$ the homogeneous degree is 4 and the (convex) zero-polytope becomes a zero-simplex.

Henceforth, I will consider pure states of four qubits, whose three qubit minors automatically have rank two, and I will consider τ_3 and $\sqrt{\tau_3}$ as entanglement measures. The threetangle τ_3 is defined as[4] (see also in refs. [14,

15, 28])

$$\begin{aligned} \tau_3 &= |d_1 - 2d_2 + 4d_3| \\ d_1 &= \psi_{000}^2 \psi_{111}^2 + \psi_{001}^2 \psi_{110}^2 + \psi_{010}^2 \psi_{101}^2 + \psi_{100}^2 \psi_{011}^2 \\ d_2 &= \psi_{000} \psi_{111} \psi_{011} \psi_{100} + \psi_{000} \psi_{111} \psi_{101} \psi_{010} \\ &\quad + \psi_{000} \psi_{111} \psi_{110} \psi_{001} + \psi_{011} \psi_{100} \psi_{101} \psi_{010} \\ &\quad + \psi_{011} \psi_{100} \psi_{110} \psi_{001} + \psi_{101} \psi_{010} \psi_{110} \psi_{001} \\ d_3 &= \psi_{000} \psi_{110} \psi_{101} \psi_{011} + \psi_{111} \psi_{001} \psi_{010} \psi_{100} \end{aligned} ,$$

In order to avoid misunderstandings, the function is highlighted whose convex roof will be calculated by a hat symbolizing the convex roof. It is worth mentioning here that the convex roofs $\widehat{\tau}_3$ of τ_3 and $\widehat{\sqrt{\tau_3}}$ of $\sqrt{\tau_3}$ are different in general; in particular we have $\widehat{\sqrt{\tau_3}}^2 \leq \widehat{\tau}_3$. In fact, for every positive invertible concave function f we have $f^{-1}(f(\tau)) \leq \widehat{\tau}$. This is because for an optimal decomposition of τ , we get with $f(\tau)$ a result, which in some points may not be convex any more. Since for calculating the convex roof, one has to convexify $f(\tau)$, and any optimal decomposition of $f(\tau)$ will lie below this result, we finally get $f^{-1}(\widehat{f(\tau)}) \leq \widehat{\tau}$.

I will consider the functions $\widehat{\sqrt{\tau_3}}$ and $\widehat{\tau}_3$ in what follows. I will sometimes call both functions *threetangle*.

THREETANGLE OF PURE FOUR-QUBIT STATES

A classification of four-qubit states has been found in Ref. [12], which can be compared to the Schmidt decomposition for two qubits and its extension for three qubits[29], where however the local transformations are out of the general linear group with non-vanishing determinant, hence not unitary in general.

Here, I present calculations that offer in general an upper bound to the threetangle. In most cases however, they provide with the exact convex roof of the threetangle for the states. I looked at all nine classes whereas discussions are only included up to class 6, since for the remaining classes 7 to 9 it is either clear that the respective threetangle vanishes, or the previously given estimate coincides with the convex roof. A good upper bound is given for class 5, where I have good reasons why the decomposition that I obtain is at least close to optimal.

The qubits are numbered as (1, 2, 3, 4) corresponding to the state $|q_1, q_2, q_3, q_4\rangle$. Please notice that the two states $|\psi_i\rangle$, $i = 1, 2$, are not normalized. All subsequent definitions are class-local.

Class 1

The representant of this class, which contains all the stochastic states[12, 14–16] with reduced local density

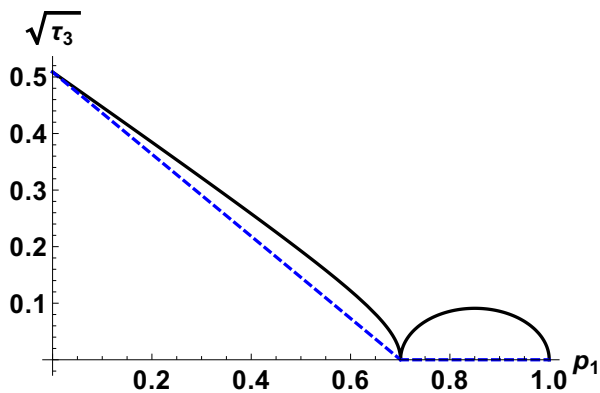


FIG. 2: The minimal characteristic curves for the angles $\varphi = \arg z_0 + j\pi$ on the Bloch sphere are shown for $j = 0, 1$ (black line) together with the convexified curve τ_3^{conv} (blue dashed line). The optimal decompositions are $|\psi_2\rangle$ and the two corresponding $|\psi_{z_0}\rangle$ for a finite value of $\sqrt{\tau_3}$, and $|\psi_1\rangle$ and the two $|\Psi_{z_0}\rangle$ for vanishing threetangle (see explanations in the text).

matrices proportional to the identity, is

$$\begin{aligned}
 |G_{abcd}^1\rangle &= \frac{a+d}{2}(|0000\rangle + |1111\rangle) \\
 &+ \frac{a-d}{2}(|0011\rangle + |1100\rangle) \\
 &+ \frac{b+c}{2}(|0101\rangle + |1010\rangle) \\
 &+ \frac{b-c}{2}(|0110\rangle + |1001\rangle) \quad (8)
 \end{aligned}$$

All three qubit minors are equivalent with respect to their eigenvalues and threetangle in their eigenstates, and we have $\tau_3[\rho] = 0$, as pointed out already in Ref. [12].

Class 2

The representant for the second class is defined as[12]

$$\begin{aligned}
 |G_{abc}^2\rangle &= \frac{a+b}{2}(|0000\rangle + |1111\rangle) \\
 &+ \frac{a-b}{2}(|0011\rangle + |1100\rangle) \\
 &+ c(|0101\rangle + |1010\rangle) + |0110\rangle, \quad (9)
 \end{aligned}$$

and the reduced three-qubit density matrices are again equivalent, in that they have the same eigenvalues and also the same threetangles of their eigenstates. Tracing out e.g. the fourth qubit, this gives rise to the two eigenstates

$$|\psi_1\rangle = (a^* - b^*)|001\rangle + (a^* + b^*)|111\rangle + 2c^*|010\rangle \quad (10)$$

$$|\psi_2\rangle = (a^* + b^*)|000\rangle + (a^* - b^*)|110\rangle + 2c^*|101\rangle + 2|011\rangle, \quad (11)$$

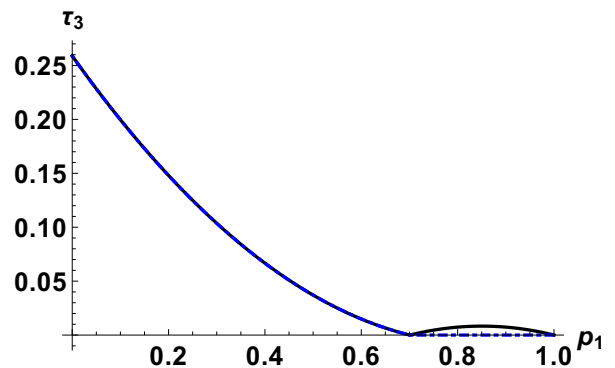


FIG. 3: A typical example for a minimal characteristic curve for τ_3 is shown (black line) together with the convexified one τ_3^{conv} (blue dashed line). Here the curve is strictly convex where the threetangle is finite. This leads to an optimal decomposition at p_1 which is $|\Psi_{\pm z(p_1)}\rangle$ and gives rise to smaller values for the convex roof $\widehat{\tau}_3$.

with the probability of $|\psi_1\rangle$ being

$$p_1(a, b, c) = \frac{|a|^2 + |b|^2 + 2|c|^2}{2(1 + |a|^2 + |b|^2 + 2|c|^2)}. \quad (12)$$

A typical example of a minimal characteristic curve is shown in figs. 2 and 3 for $\sqrt{\tau_3}$ and τ_3 , respectively. The convexified minimum of the characteristic curves (blue dashed line), $\sqrt{\tau_3^{conv}}(p_1)$ and $\tau_3^{conv}(p_1)$, are also plotted. A decomposition of a convexified region is always given by the corresponding states $|\Psi_{z_0}\rangle$, which flank the region. The zero simplex is flanked by two trivial zeros at $p_1 = 1$ ($z = 0$) and the two values

$$\begin{aligned}
 z_0 &= \pm \frac{1}{2} \sqrt{\frac{2 + |a-b|^2 + 2|c|^2}{|a|^2 + |b|^2 + 2|c|^2}} \\
 &\times \sqrt{\frac{b^2}{c} \left(1 + \frac{c^2 a(a-b) + c^2}{b^2 (a-b)^2} \right)^*}, \quad (13)
 \end{aligned}$$

and hence $p_0 = 1/(1 + |z_0|^2)$. Whereas for τ_3 the only convexified region is inside the zero-simplex[19, 20] in the interval $[p_0, 1]$, for $\sqrt{\tau_3}$ it is given additionally by a straight line connecting the threetangle at $p = 0$ with the beginning of the zero-simplex at p_0 . Hence, the convex roof $\widehat{\sqrt{\tau_3}}$ of $\sqrt{\tau_3}$ is

$$\widehat{\sqrt{\tau_3}} = \max \left\{ 0, 2\sqrt{\frac{|(a^2 - b^2)c|}{1 + |a|^2 + |b|^2 + 2|c|^2}} \left(1 - \frac{|a|^2 + |b|^2 + 2|c|^2}{2p_{0;2}(1 + |a|^2 + |b|^2 + 2|c|^2)} \right) \right\}, \quad (14)$$

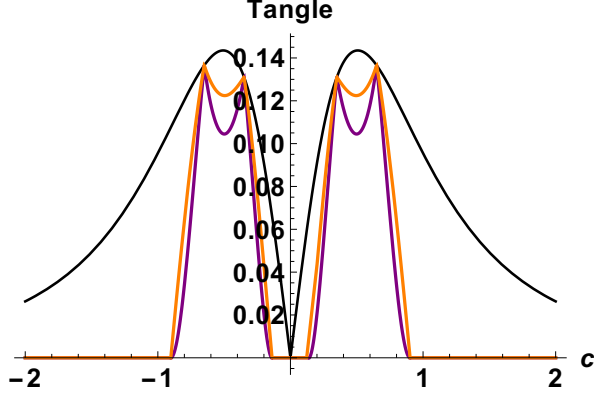


FIG. 4: Class 2: The convex roofs are shown for $\widehat{\tau}_3$ (central orange curve) and $\widehat{\sqrt{\tau_3}}^2$ (lower purple curve) for real values of $a = 0.65$, $b = 0.35$ and c . It is seen that $\widehat{\sqrt{\tau_3}}^2 < \widehat{\tau}_3$. For comparison we plot also the curve obtained by Ref. [27] from the algorithm suggested in Ref. [26] (upper black curve). They coincide at the pikes of the curves, where the convex roof is given by the eigen-decomposition.

and the optimal decomposition in between $p_1 = 0$ and p_0 is made of the eigenstate at $|\psi_2\rangle$ and the two states at $|\Psi_{\pm z_0}\rangle$. For τ_3 instead, we obtain that the minimal characteristic curve is convex in $[p_1 = 0, p_0]$, and hence the optimal decomposition is given here in terms of $|\Psi_{z(p)}\rangle$ and $|\Psi_{-z(p)}\rangle$ between $p_1 = 0$ and p_0 . [34] Whereas we managed to give a closed formula for the convex roof $\widehat{\sqrt{\tau_3}}$, we here give $\widehat{\tau}_3$ only in the implicit form

$$\widehat{\tau}_3 = \max\{0, \tau_3^{conv}(p_1(a, b, c))\}, \quad (15)$$

with the convexification $\tau_3^{conv}(p_1)$ of $\tau_3(p_1)$.

To illustrate the convex roofs, we show $\widehat{\sqrt{\tau_3}}^2$ and $\widehat{\tau}_3$ for $a = 0.65$, $b = 0.35$ in fig. 4 as a function of a real c . The two convex roofs are seen to rise sharply at $c = \pm 0.1388$ and vanish again at $c = \pm 0.9022$ with two cusps at $c = \pm 0.35$ with values $\widehat{\tau}_3 = 0.1311$, and at $c = 0.65$ with value $\widehat{\tau}_3 = 0.1366$. Here, the characteristic curves become straight lines for $\sqrt{\tau_3}$ and the corresponding parabolas for τ_3 . Hence, both convex roofs coincide here. For comparison we show the curve from [27, 30]

$$\widehat{\sqrt{\tau_3}}^2 = 4 \frac{|(a^2 - b^2)c|}{(1 + |a|^2 + |b|^2 + 2|c|^2)^2} \quad (16)$$

which is an upper bound to $\widehat{\sqrt{\tau_3}}^2$, as it should be. It clearly overestimates the thretriangle in the state except

at the cusps at $c = \pm a$ and $c = \pm b$, where all zeros z_0 coincide.

Class 3

The representant of the third class is given by[12]

$$\begin{aligned} |G_{ab}^3\rangle &= a(|0000\rangle + |1111\rangle) \\ &+ b(|0101\rangle + |1010\rangle) \\ &+ |0110\rangle + |0011\rangle \end{aligned} \quad (17)$$

There are two inequivalent three-qubit density matrices with respect to their eigenvalues and thretriangle here. The thretriangle vanishes for two of these density matrices (qubits numbers 2 and 4 traced out). The eigenstates of the remaining reduced density matrices (here: qubit 1 traced out) are

$$|\psi_1\rangle = b^*|010\rangle + a^*|111\rangle \quad (18)$$

$$|\psi_2\rangle = a^*|000\rangle + b^*|101\rangle + |011\rangle + |110\rangle \quad (19)$$

and the typical characteristic curves have mainly the same form as for class 2, and are therefore not shown. The weight of $|\psi_1\rangle$ in the density matrix is

$$p_1(a, b) = \frac{|a|^2 + |b|^2}{2(1 + |a|^2 + |b|^2)}. \quad (20)$$

We consider again solutions to

$$\tau_3 \left(\frac{|\psi_1\rangle}{\|\psi_1\rangle} + z \frac{|\psi_2\rangle}{\|\psi_2\rangle} \right) = 0 \quad (21)$$

which has zeros at

$$z_0 = \pm i \left(\frac{a^2 - b^2}{2\sqrt{ab}} \right)^* \sqrt{\frac{2 + |a|^2 + |b|^2}{|a|^2 + |b|^2}} \quad (22)$$

and corresponding values for p_0 . This leads to the following convex roof of $\sqrt{\tau_3}$

$$\widehat{\sqrt{\tau_3}} = \max \left\{ 0, \frac{4|ab| - |a^2 - b^2|^2}{2\sqrt{|ab|(1 + |a|^2 + |b|^2)}} \right\}. \quad (23)$$

The corresponding thretriangles $\widehat{\sqrt{\tau_3}}^2$ and $\widehat{\tau}_3$ are shown for $a = 2.0$ in fig. 5, where it is seen that $\widehat{\sqrt{\tau_3}}^2 < \widehat{\tau}_3$ except for the points $b \approx \pm 1.0498$ and $b \approx \pm 2.9804$, where the thretriangle vanishes, and at $b = \pm 2.0$, where

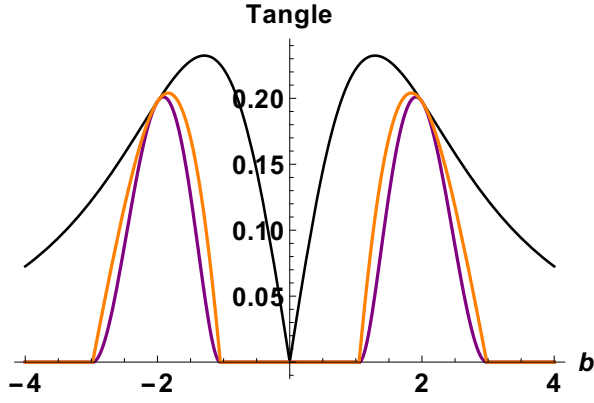


FIG. 5: Class 3: The convex roofs $\widehat{\tau}_3$ (central orange curve) and $\widehat{\sqrt{\tau_3}}^2$ (lower purple curve) are shown together with the estimate of Ref. [27] (upper black curve) for $a = 2.0$. It can be seen that they both coincide at $a = b = 2.0$, where the minimal characteristic curve of $\widehat{\sqrt{\tau_3}}$ is a straight line. At this point, it also must coincide with the estimate in Ref. [27], which highly overestimates the convex roofs. The optimal decompositions are made out of $|\Psi_{\pm z_0}\rangle$ and $|\psi_2\rangle$ for a finite $\widehat{\sqrt{\tau_3}}$, and $|\Psi_{\pm z(p_1)}\rangle$ for finite $\widehat{\tau}_3$.

the characteristic curve of $\sqrt{\tau_3}$ again reduces to a straight line and the zeros z_0 coincide. At this latter points the convex roof again coincides with the upper bound of [27], since the method of ref. [26] gives the exact convex roof here. It is seen however that in general the estimate taken from [27] considerably overestimates the threetangle of the state.

Class 4

The class 4 is represented by[12]

$$\begin{aligned}
 |G_{ab}^4\rangle &= a(|0000\rangle + |1111\rangle) + \frac{a+b}{2}(|0101\rangle + |1010\rangle) \\
 &+ \frac{a-b}{2}(|0110\rangle + |1001\rangle) \\
 &+ \frac{i}{\sqrt{2}}(|0001\rangle + |0010\rangle + |0111\rangle + |1011\rangle) \quad (24)
 \end{aligned}$$

Also here, all four reduced density matrices are equivalent with respect to their eigenvalues and threetangle of their eigenstates. A set of eigenstates of one of the reduced three-qubit density matrix (qubit number 1 traced out)

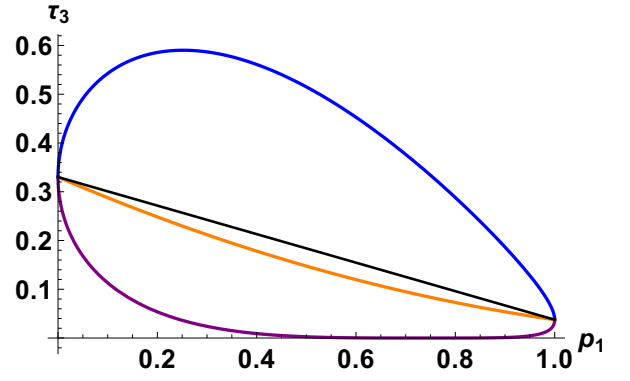


FIG. 6: Some characteristic curves are shown for real values $a = 0.4$, $b = 1.9$ and angles $\varphi = \pi$ (the minimum; lower purple curve), $\varphi = \pm\pi/2$ (central orange curve), and $\varphi = 0$ (the maximum; upper blue curve). For comparison the straight line (thin black curve) marks the convex combination of the two eigenstates. There is a single zero of fourth order at $z = -|\psi_2\rangle/|\psi_1\rangle$ of the equation $\tau_3(|\psi_1\rangle/|\psi_1\rangle + z|\psi_2\rangle/|\psi_2\rangle) = 0$.

is

$$\begin{aligned}
 |\psi_1\rangle &= i\sqrt{2}a^*s_-|000\rangle + (s_- - 2a(a^* - b^*))|001\rangle \\
 &+ (s_- - 2a(a^* + b^*))|010\rangle + 2i\sqrt{2}a|011\rangle \\
 &+ \frac{i}{\sqrt{2}}s_-(a^* + b^*)|101\rangle \quad (25) \\
 &+ \frac{i}{\sqrt{2}}s_-(a^* - b^*)|110\rangle + (s_- - 4|a|^2)|111\rangle \\
 |\psi_2\rangle &= i\sqrt{2}a^*s_+|000\rangle + (s_+ + 2a(a^* - b^*))|001\rangle \\
 &+ (s_+ + 2a(a^* + b^*))|010\rangle - 2i\sqrt{2}a|011\rangle \\
 &+ \frac{i}{\sqrt{2}}s_+(a^* + b^*)|101\rangle \quad (26) \\
 &+ \frac{i}{\sqrt{2}}s_+(a^* - b^*)|110\rangle + (s_+ + 4|a|^2)|111\rangle,
 \end{aligned}$$

where $s_{\pm} = \sqrt{1 + 8|a|^2} \pm 1$, with a typical set of characteristic curves shown in fig. 6 and 7 for τ_3 and $\sqrt{\tau_3}$, respectively. The weight of $|\psi_1\rangle$ is

$$p_1(a, b) = \frac{2 + 3|a|^2 + |b|^2 - \sqrt{1 + 8|a|^2}}{4 + 6|a|^2 + 2|b|^2}. \quad (27)$$

We show the minimal curve in purple (at $\varphi = \pi$), the two identical central curves in orange ($\varphi = \pm\pi/2$), and the maximum ($\varphi = 0$, blue curve). There is a four-fold degeneracy of the solution to the equation $\tau_3(|\psi_1\rangle/|\psi_1\rangle + z|\psi_2\rangle/|\psi_2\rangle) = 0$, which is $z_0 = -|\psi_2\rangle/|\psi_1\rangle$; it corresponds to $p_0 = |\psi_1\rangle/(|\psi_1\rangle + |\psi_2\rangle)$.

It is worth mentioning that the minimal characteristic curve can impossibly constitute the minimum of decompositions of ρ , because it had to be combined with curves beyond the $\varphi = \pm\pi/2$ lines to this end. One possibility is to combine it with the curve at $\varphi = 0$ in order to give a decomposition of ρ , which is the maximal curve,

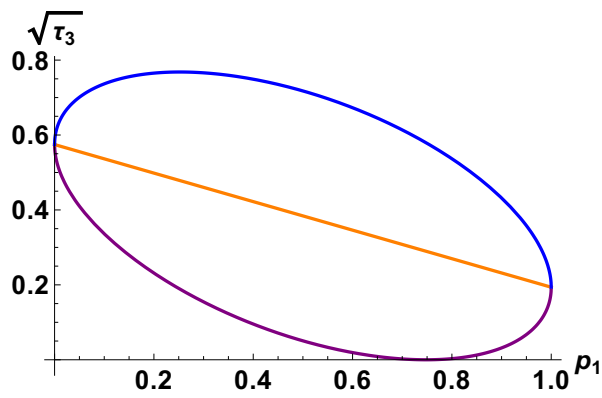


FIG. 7: The minimal (lower purple curve) and maximal (upper blue curve) characteristic curves are shown here for real $a = 0.4$ and $b = 1.9$ and the same angles as in fig. 6. The curves at $\varphi = \pm\pi/2$ coincide and possibly even give the convex roof result. Here, this is a straight line connecting both eigenstates, and consequently also the algorithm of Ref. [26] gives this result.

though. In this case the result for $\sqrt{\tau_3}$ (fig. 7) is the same as the central orange curves at $\varphi = \pm\pi/2$. This does not change, when whatever $q_i \in [0, 1]$ is taken as defining the decomposition at an arbitrary angle. In fact, in the case of coinciding zeros z_0 it has been shown during the publication process of this work[31] that the exact convex roof is obtained for $\widehat{\sqrt{\tau_3}}$, and that all decompositions of ρ are optimal.

Therefore we conclude that $\widehat{\sqrt{\tau_3}}^2$ as well as $\widehat{\tau_3}$ is given by

$$\widehat{\sqrt{\tau_3}}^2 = \widehat{\tau_3} = \max\left\{0, 2\frac{|a^2 - b^2|}{2 + 3|a|^2 + |b|^2}\right\}. \quad (28)$$

We want to mention however that the real outcome of the analysis of Ref. [27] is that consequently the residual tangle is larger than a negative value, due to violations in this class 4 only. In ref. [27] instead, it was not known that it was the convex roof for that class, and the authors could at best say that an extended monogamy clearly guarantees positivity of the residual tangle. This changes with the Ref. [31] in which it is clearly demonstrated to be the convex roof.

We show the values for $\widehat{\tau_3}$ and $\widehat{\sqrt{\tau_3}}^2$ for real values of a and b in fig. 8.

Class 5

The representant of the fifth class is given by[12]

$$|G_a^5\rangle = a(|0000\rangle + |1111\rangle + |0101\rangle + |1010\rangle) + i(|0001\rangle - |1011\rangle + |0110\rangle) \quad (29)$$

The reduced three-qubit density matrices are all equivalent with respect to the eigenvalues. But there are two

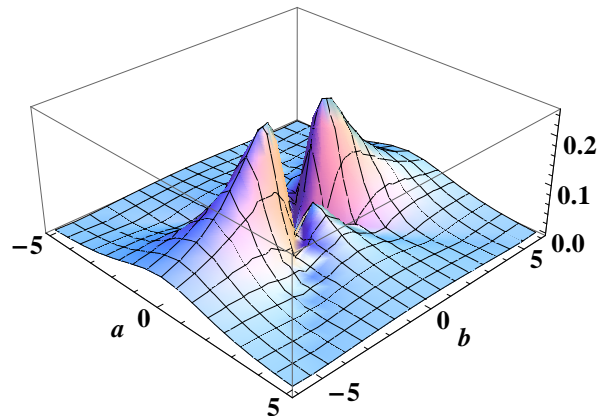


FIG. 8: The values for $\widehat{\tau_3} = \widehat{\sqrt{\tau_3}}^2$ in class 4 for real values of a and b .

inequivalent subsets when looking at the threetangles of their eigenstates. The corresponding set of eigenstates of one of the reduced three-qubit density matrices is

$$|\psi_{1,1}\rangle = -i|000\rangle + a^*|010\rangle + i|101\rangle + a^*|111\rangle \quad (30)$$

$$|\psi_{1,2}\rangle = a^*|000\rangle + |011\rangle + a^*|101\rangle \quad (31)$$

when qubit number 4 (this is equivalent to tracing out qubit number 2) is traced out, and

$$|\psi_{2,1}\rangle = |010\rangle + a^*|100\rangle + i|101\rangle + a^*|111\rangle \quad (32)$$

$$|\psi_{2,2}\rangle = a^*|000\rangle - i|001\rangle + a^*|011\rangle \quad (33)$$

when tracing out qubit number 3. The weight or probability of the states $|\psi_{1,1}\rangle$ and $|\psi_{2,1}\rangle$ is

$$p_1(a) = \frac{2(1 + |a|^2)}{3 + 4|a|^2}. \quad (34)$$

We will consider the former case first. The solution for the zero-simplex is a four-fold zero at $z = 0$ here corresponding to a solution for the convex roof of

$$\widehat{\tau_3} = \widehat{\sqrt{\tau_3}}^2 = 16\frac{|a|^2}{(3 + 4|a|^2)^2}, \quad (35)$$

which naturally is the same as the estimate of Ref. [27].

The latter case is more interesting, and is given by the characteristic curves, which I show in fig. 9. Here is a threefold degenerate solution for the zero-simplex at $z = 0$ and a single solution at $z_0 = 8\sqrt{2}i(a^*)^2\sqrt{\frac{1+|a|^2}{1+2|a|^2}}$ to $\tau_3(z|\psi_{2,1}\rangle/|\psi_{2,1}\rangle + |\psi_{2,2}\rangle/|\psi_{2,2}\rangle) = 0$, which corresponds to the probability

$$p_0 = 1 - \frac{1}{1 + |z_0|^2} = \frac{128|a|^4(1 + |a|^2)}{1 + 2|a|^2 + 128|a|^4(1 + |a|^2)}. \quad (36)$$

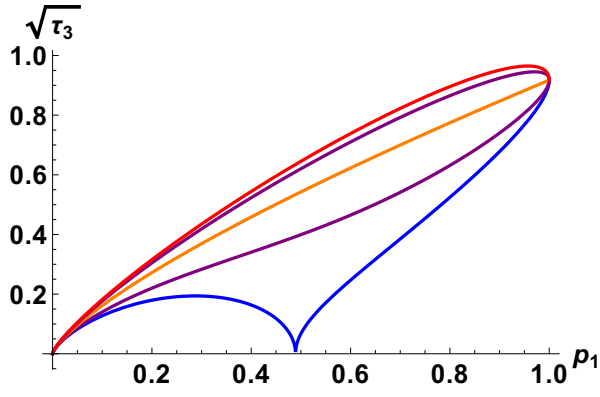


FIG. 9: For real value $a = 0.3$ among some characteristic curves are shown in particular the minimal characteristic curve at $\varphi = \pi/2$ (lower blue line) and maximal characteristic curve at $\varphi = 3\pi/2$ (higher red curve) and the two intermediate coinciding curves at $\varphi = 0, \pi$ (central orange curve).

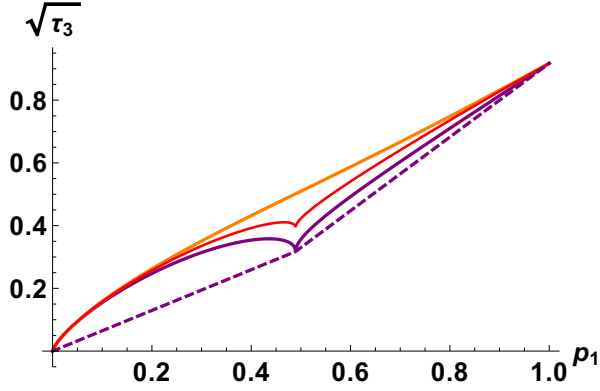


FIG. 10: For $a = 0.3$ the sum of two by an angle of π differing characteristic curves are shown for $\varphi = 0, \pi$ (higher orange curve) and for $\varphi = \pi/2, 3\pi/2$ (lower purple curve), combining to possible decompositions of ρ . The convexification of this latter curve is also shown (purple dashed line). A decomposition into three states (thin red curve) is shown to be situated between the lower purple and higher orange curve.

The results for certain decompositions of ρ are shown in fig. 10. At first, I am considering the decompositions out of the two states at angles $\varphi = \pm\pi/2$ (lowest purple curve) and at $\varphi = 0, \pi$ (highest orange curve) at a given p_1 . The combination of three states with phases $\varphi = 3i\pi/2 + 2mi\pi/3$ for $m = 0, 1, 2$ (red curve) is shown to lie in between the purple and the orange curve.

Another choice is, to combine the state at p_0 at $\varphi = \pi/2$ with another state at the angle $\varphi = 3\pi/2$ and q . Any two such states form a decomposition for $\rho(p_1) = p_1|\psi_{2,1}\rangle\langle\psi_{2,1}| + (1 - p_1)|\psi_{2,2}\rangle\langle\psi_{2,2}|$ with some $p_1(q)$, giving a value for $\sqrt{\tau_3}(p_1)$ which is shown in fig. 11. This curve is convex (lowest black curve in fig. 11) and always below the preceding convexified minimal curve (dashed purple curve), except at p_0 and at $p_1 = 0, 1$, where it coincides with it. [35] Each curve corresponding

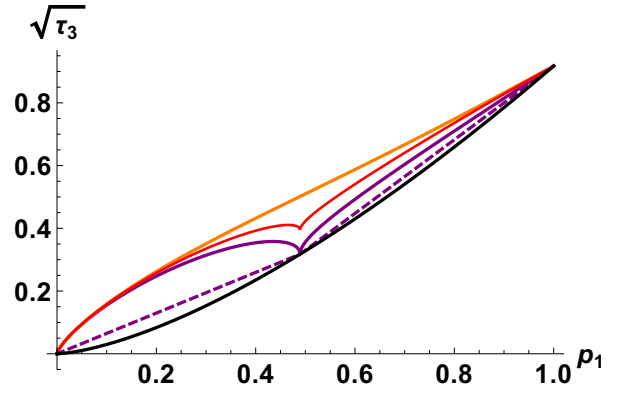


FIG. 11: In addition to figure 10, convex combinations of the state $|\Psi_{z_0}\rangle$ with a second state at $\varphi = \pi/2$ to give a decomposition of $\rho(p_1)$ are shown in the convex lower black curve. Every combination from the zero-simplex with another state at $\varphi = \pi/2$ lies above this curve. This is the lowest upper bound. I conjecture that it equals the convex roof.

to a sum of some pure state at q_0 on the minimal characteristic curve at $\varphi = \pi/2$ and the to $\rho(p_1)$ corresponding pure state at $3\pi/2$ is lying above this curve and this does not change if choosing some other angle φ . It is furthermore the minimal curve of superpositions of a (in general mixed) state inside the zero-simplex at $\varphi = \pi/2$ and a corresponding pure state to $\rho(p_1)$ at $\varphi = 3\pi/2$. It will therefore constitute a reasonable upper bound. I conjecture that it coincides with the convex roof.

I have calculated for this upper bound of $\widehat{\sqrt{\tau_3}}$ the entanglement in the state $|G^5(a)\rangle$ to be

$$\widehat{\sqrt{\tau_3}}^2 \leq 4 \frac{1 + 64|a|^2}{((3 + 4|a|^2)(1 + 64|a|^4))^2} \quad (37)$$

$$< \frac{4}{(3 + 4|a|^2)^2}, \quad (38)$$

which is plotted in fig. 12. For τ_3 I get the implicit version

$$\widehat{\tau_3} \leq \min\{0, \tau_3^{conv}(p_1(a))\}. \quad (39)$$

It can be seen that the new upper bound (37) is considerably better than that previously published in Ref. [27], and given by Eq. (38).

I want to mention that in calculating the curve for τ_3 I did not consider the convexified version of the corresponding curve τ_3^{conv} . This would give a smaller result for the states under consideration. So while I conjectured that for $\sqrt{\tau_3}$ I have the convex roof, this certainly isn't so for τ_3 . But I find it curious that it coincides with the upper bound in Ref. [27] for $\widehat{\sqrt{\tau_3}}^2$.

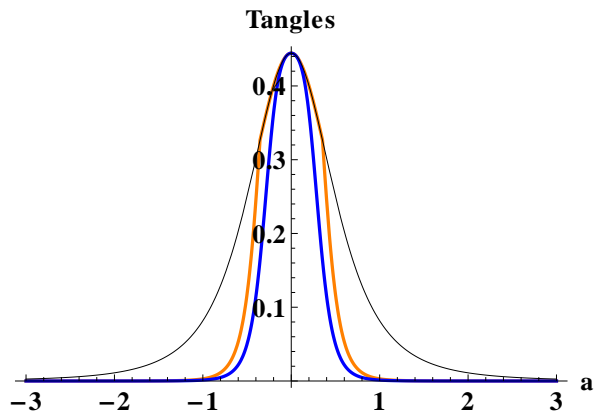


FIG. 12: Class 5 for qubits 1 or 3 traced out: Upper bounds for $\widehat{\tau}_3^2$ (which is the conjectured convex roof; lower blue curve) and $\widehat{\tau}_3$ (central orange curve) are shown in this figure. They are compared with the result in Ref. [27] (upper black curve) making use of the algorithm related to Ref. [26]. It is seen, that it overestimates the value for $\widehat{\tau}_3$. It astonishingly coincides for small values of a with the upper bound for $\widehat{\tau}_3$, but then deviates from it. This coincidence is due to not having calculated the upper bound for the convexification of the corresponding minimal curve that I have found. It is nicely seen that the upper bounds satisfy the inequality $\widehat{\tau}_3^2 < \widehat{\tau}_3$ for the convex roofs.

Class 6

The representant of the fifth class is given by[12]

$$|G_a^6\rangle = a(|0000\rangle + |1111\rangle) + |0011\rangle + |0101\rangle + |0110\rangle \quad (40)$$

The reduced three qubit density matrix has non-vanishing threetangle only, when tracing out the first qubit; it gives zero threetangle in the remaining cases. The typical characteristic curves for the non-vanishing case have the same structure as in class 2, and are hence not shown here. The interesting eigenstates are

$$|\psi_1\rangle = |111\rangle \quad (41)$$

$$|\psi_2\rangle = a^*|000\rangle + |011\rangle + |101\rangle + |110\rangle, \quad (42)$$

and the weight of $|\psi_1\rangle$ is $p_1(a) = |a|^2/(3 + 2|a|^2)$. The solutions for the zero-simplex are given by two trivial zeros $z = 0$, and

$$z_0 = \pm \frac{1}{2} \sqrt{a^*(3 + |a|^2)}. \quad (43)$$

The convex roofs are obtained in the same way as for class 2 before. For $\widehat{\tau}_3^2$ we obtain

$$\widehat{\tau}_3^2 = \max\left\{0, \frac{|a|(|a|^3 - 4)^2}{(2|a|^2 + 3)^2}\right\}, \quad (44)$$

and for $\widehat{\tau}_3 = \max\{0, \tau_3^{conv}(p_1(a))\}$ we get an implicit result. The threetangles of the state are shown in fig.13.

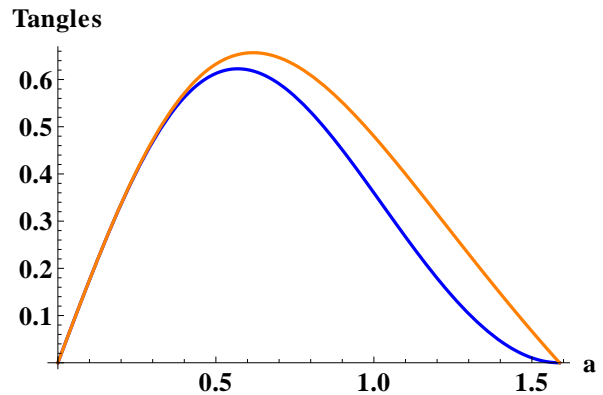


FIG. 13: Class 6: Both convex roofs $\widehat{\tau}_3^2$ (blue lower curve) and $\widehat{\tau}_3$ (orange curve) are shown. It is seen that $\widehat{\tau}_3^2 \leq \widehat{\tau}_3$. Both values vanish if $|a| \geq 2^{2/3}$. It is strange that the upper bound from Ref. [27] coincides with $\widehat{\tau}_3^2$, where instead something larger would be expected. This appears to be accidental and could be interrelated with only two apparent solutions to the zero-simplex, when the z appears in front of a state with zero threetangle.

Surprisingly, here the upper bound obtained in Ref. [27] coincides with the convex roof solution $\widehat{\tau}_3^2$ whereas the zeros indicate that the result should be actually bigger. This strange coincidence could have been caused by ignoring the two trivial zeros.

For the remaining classes, the estimates in Ref. [27] from the algorithm in Ref. [26] are precisely the convex roof measure for $\widehat{\tau}_3^2$ which coincides with $\widehat{\tau}_3$ in these cases.

CONCLUSIONS

I have classified four-qubit pure states with respect to their mixed threetangle. In order to do so, I have taken the representatives of the nine SL-classes from Ref. [12]. Those for general four-qubit states can be obtained by acting with SL operations on the four qubits and considering that the threetangle is an SL invariant[23]. Whereas the convex roof could be obtained in 8 out of 9 classes in finding an optimal decomposition, for class 5 better upper bounds than those existing in Ref. [27] could be given. There are strong indicators that it is at least close to the convex roof. I compare the results with a method related to that published in Ref. [26] that has been used to obtain upper bounds in Ref. [27, 30] and found that the method gives the exact value for the threetangle in cases where the four solutions of the zero-simplex do coincide. In these cases already the eigen-decomposition provides the convex roof. Away from these points, the convex roof is considerably below this estimate. For class 2, the upper bound of Ref. [27] has

been corrected[30] and fits nicely as an upper bound with my findings. Finally, due to Ref. [31] which shows that the upper bound obtained in Ref. [27] coincides with the convex-roof, the strong monogamy strictly has to be applied (see also Ref. [32]).

Acknowledgements

During the completion of this work, I had intense and fruitful discussion with G. Adesso and B. Regula.

* Electronic address: andreas.osterloh@uni-due.de

- [1] S. Hill and W. K. Wootters, Phys. Rev. Lett. **78**, 5022 (1997).
- [2] W. K. Wootters, Phys. Rev. Lett. **80**, 2245 (1998).
- [3] A. Uhlmann, Open Syst. Inf. Dyn. **5**, 209 (1998), quant-ph/9704017.
- [4] V. Coffman, J. Kundu, and W. K. Wootters, Phys. Rev. A **61**, 052306 (2000).
- [5] T. J. Osborne and F. Verstraete, Phys. Rev. Lett. **96**, 220503 (2006).
- [6] W. Dür, G. Vidal, and J. I. Cirac, Phys. Rev. A **62**, 062314 (2000).
- [7] G. Vidal, J. Mod. Opt. **47**, 355 (2000).
- [8] A. Peres, Phys. Rev. Lett. **77**, 1413 (1996).
- [9] M. Horodecki, P. Horodecki, and R. Horodecki, Phys. Lett. A **223**, 1 (1996).
- [10] G. Vidal and R. F. Werner, Phys. Rev. A **65**, 032314 (2002).
- [11] B. Jungnitsch, T. Moroder, and O. Gühne, Phys. Rev. Lett. **106**, 190502 (2011).
- [12] F. Verstraete, J. Dehaene, B. De Moor, and H. Verschelde, Phys. Rev. A **65**, 052112 (2002).
- [13] F. Verstraete, J. Dehaene, and B. De Moor, Phys. Rev. A **65**, 032308 (2002).
- [14] F. Verstraete, J. Dehaene, and B. De Moor, Phys. Rev. A **68**, 012103 (2003).
- [15] A. Osterloh and J. Siewert, Phys. Rev. A **72**, 012337 (2005).
- [16] A. Osterloh and J. Siewert, Int. J. Quant. Inf. **4**, 531 (2006).
- [17] D. Ž. Đoković and A. Osterloh, J. Math. Phys. **50**, 033509 (2009).
- [18] G. Gour and N. R. Wallach, J. Math. Phys. **51**, 112201 (2010).
- [19] R. Lohmayer, A. Osterloh, J. Siewert, and A. Uhlmann, Phys. Rev. Lett. **97**, 260502 (2006).
- [20] A. Osterloh, J. Siewert, and A. Uhlmann, Phys. Rev. A **77**, 032310 (2008).
- [21] E. Jung, M.-R. Hwang, D. Park, and J.-W. Son, Phys. Rev. A **79**, 024306 (2009).
- [22] H. Shu-Juan, W. Xiao-Hong, F. Shao-Ming, S. Hong-Xiang, and W. Qiao-Yan, Comm. Theor. Phys. **55**, 251 (2011).
- [23] O. Viehmann, C. Eltschka, and J. Siewert, Appl. Phys. B **106**, 533 (2012), spring Meeting of the German-Physical-Society, Dresden, GERMANY, 2011.
- [24] C. Eltschka and J. Siewert, Phys. Rev. Lett. **108**, 020502 (2012).
- [25] J. Siewert and C. Eltschka, Phys. Rev. Lett. **108**, 230502 (2012).
- [26] S. Rodrigues, N. Datta, and P. Love, Phys. Rev. A **90**, 012340 (2014).
- [27] B. Regula, S. D. Martino, S. Lee, and G. Adesso, Phys. Rev. Lett. **113**, 110501 (2014).
- [28] A. Wong and N. Christensen, Phys. Rev. A **63**, 044301 (2001).
- [29] A. Acín, A. Andrianov, L. Costa, E. Jane, J. Latorre, and R. Tarrach, Phys. Rev. Lett. **85**, 1560 (2000).
- [30] B. Regula, S. D. Martino, S. Lee, and G. Adesso, Phys. Rev. Lett. **116**, 049902 (2016), erratum.
- [31] B. Regula and G. Adesso, Phys. Rev. Lett. **116**, 070504 (2016).
- [32] B. Regula, A. Osterloh, and G. Adesso (2016), arXiv:1604.03419.
- [33] A zero-polytope is made out of those pure states on which E vanishes. It has been called *zero-simplex* in refs. [19, 20]. Every such zero-polytope is made of zero-simplices of $d + 1$ points in d dimensions.
- [34] Here, with $z(p_1)$ I mean that $\arg z = \arg z_0$ of the solutions z_0 of $E(z) = 0$ ($E = \tau_3$ here), since here the minimal characteristic curve does not depend on $\arg z = \varphi$.
- [35] Note that this must not be confused with the convex characteristic curve, which of course lies below this curve.